Enhanced Oceanic Environmental Responses and Feedbacks to Super Typhoon Nida (2009) during Sudden-turning Stage

Jiagen Li[1], Yuanjian Yang[2], Guihua Wang[3], Hao Cheng[1], and Liang Sun[4]

[1]University of Science and Technology of China
[2]Nanjing University of Information Science & Technology
[3]Fudan University
[4]School of Earth and Space Sciences, University of Science and Technology of China

November 24, 2022

Abstract

The ocean surface and subsurface biophysical responses and their feedbacks to super typhoon Nida (2009) are investigated. Nida experienced two Category 5 stages: a rapid intensification stage that was fast moving along a straight-line track, and a rapid weakening stage that was slow moving along a sharp-left sudden-turning track. In the first Category 5 stage, Nida caused an average sea surface temperature (SST) cooling of -1.44 , a sea surface height anomalies (SSHAs) decrease of -5.00 cm and a chlorophyll-a (chl-a) concentration increase of 0.03 mg m-3. During the second Category 5 stage, Nida induced a strong cold cyclonic eddy (SSHA $<$ -60 cm) by strong upwelling due to the slow speed of the sudden-turning track, which caused the maximum SST cooling of 6.68 , a sea surface salinity increase of 0.6 psu, a long-lasting chl-a bloom that exceeded 0.6 mg m-3 and the Kuroshio Current strengthening of 0.25 Sv, resulting in substantial impacts on the ocean ecological environment. Furthermore, the enhanced ocean cold wake and the longer air-sea interaction in turn decreased the average inner-core SST of -4 {degree sign}C and the corresponding enthalpy flux of -780 W m-2, which induced a notable negative feedback to the typhoon intensity by weakening it from Category 5 to Category 2. Our findings provide positive evidence that enhanced oceanic environmental responses and feedbacks can occur under sudden-turning and/or lingering tracks, providing insight to ocean-typhoon interactions.

Enhanced Oceanic Environmental Responses and Feedbacks to Super Typhoon Nida (2009) during Sudden-turning Stage

Jiagen Li[1], Yuanjian Yang[2,3], Guihua Wang[4], Hao Cheng[1], Liang Sun[1*]

[1]School of Earth and Space Sciences, University of Science and Technology of China, Hefei, China

[2]School of Atmospheric Physics, Nanjing University of Information Science and Technology, Nanjing, China

[3]Guangdong Key Laboratory of Ocean Remote Sensing, South China Sea Institute of Oceanology, Chinese Academy of Sciences, Guangzhou, China

[4]Department of Atmospheric and Oceanic Sciences, Fudan University, Shanghai, China

[*]Corresponding authors: Liang Sun (sunl@ustc.edu.cn)

Key Points:

- Nida generated a strong cold eddy on the left side of track during its slow-moving stage along a sharp-left sudden-turning track.
- Within the strong cold eddy, the upper ocean bio-physical responses were about 3-5 times larger than that before and lasted for weeks.
- The negative feedbacks over cold eddy in turn weakened the typhoon intensity from Category 5 to Category 2.

Abstract

The ocean surface and subsurface biophysical responses and their feedbacks to super typhoon Nida (2009) are investigated. Nida experienced two Category 5 stages: a rapid intensification stage that was fast moving along a straight-line track, and a rapid weakening stage that was slow moving along a sharp-left sudden-turning track. In the first Category 5 stage, Nida caused an average sea surface temperature (SST) cooling of −1.44 °C, a sea surface height anomalies (SSHAs) decrease of −5.00 cm and a chlorophyll-*a* (chl-*a*) concentration increase of 0.03 mg m^{-3}. During the second Category 5 stage, Nida induced a strong cold cyclonic eddy (SSHA < −60 cm) by strong upwelling due to the slow speed of the sudden-turning track, which caused the maximum SST cooling of 6.68 °C, a sea surface salinity increase of 0.6 psu, a long-lasting chl-*a* bloom that exceeded 0.6 mg m^{-3} and the Kuroshio Current strengthening of 0.25 Sv, resulting in substantial impacts on the ocean ecological environment. Furthermore, the enhanced ocean cold wake and the longer air-sea interaction in turn decreased the average inner-core SST of −4 °C and the corresponding enthalpy flux of −780 W m^{-2}, which induced a notable negative feedback to the typhoon intensity by weakening it from Category 5 to Category 2. Our findings provide positive evidence that enhanced oceanic environmental responses and feedbacks can occur under sudden-turning and/or lingering tracks, providing insight to ocean-typhoon interactions.

Plain Language Summary

The tropical cyclones of the West Pacific, namely, typhoons, can induce strong ocean surface and subsurface physical and biological responses, such as sea surface temperature (SST) cooling and chlorophyll-a blooming. In turn, the SST cooling induced by typhoon will have a negative feedback to typhoon's intensity itself. In the actual ocean, the ocean environment, typhoon track and typhoon intensity are changeable. In particular, some typhoons turn sharply during their passage, which introduces new changing factors into study the typhoon-ocean interaction process. Based on super typhoon Nida (2009), our findings provide positive evidence that enhanced oceanic environmental responses and feedbacks can occur under sudden-turning and/or lingering tracks, providing insight to ocean-typhoon interactions.

1 Introduction

It is well known that typhoons can cause notable dynamical responses of the upper ocean. The most significant one might be right-bias cold wake along typhoon track (Price, 1981) due to vertical mixing and upwelling (Walker et al., 2005; Wang et al., 2016) which transport cooler and higher-salinity seawater to the surface (Chacko, 2018; Liu et al., 2020). Within the cold wake, there may also be the marine phytoplankton blooming (Lin et al., 2003; Liu et al., 2019; Shang et al., 2008).

Since the cold wake caused by a typhoon can cool the SST (Stramma et al., 1986), it may have a negative feedback effect on the passing typhoon (Emanuel, 1986). However, there is a long-term debate whether such cold wake can immediately induce a significant negative feedback on the typhoon intensity itself (Emanuel, 2018). For example, Chang & Anthes (1979) concluded that the cold wake does not significantly affect the intensity of the typhoon itself under a typical moving speed, but Sutyrin & Khain (1984) suggested that the cold wake could induce a significant negative feedback effect on the typhoon intensity.

In general, the ocean’s negative feedback to typhoon intensity first requires that the typhoon can cause significant SST cooling. This is because the decrease in SST, especially the inner-core SST change, has a substantial impact on the observed typhoon intensity (Cione & Uhlhorn, 2003). Emanuel (1999) suggested that when the inner-core SST drops by 2.5 °C, the storm could terminate, and even a drop of 0.5 °C would have a substantial impact on the storm intensity. Second, the negative feedback of the ocean to typhoon intensity also requires the condition that the typhoon has a long residence time over the SST cooling area. As there is a lag time in the response of a typhoon to the SST (Change & Anthes, 1979; Cione & Uhlhorn, 2003; Ma et al., 2020), it needs sufficient time to feel the cold wake. Therefore, the speed of a typhoon (Lin et al., 2009) and forcing time (Sun et al., 2010) become important factors, and other related factors include SST, ocean mixed-layer depth (MLD), ocean stratification, typhoon size, latitude, and so on (Schade & Emanuel, 1999).

Although these theoretical studies are instructive for understanding the ocean-typhoon negative feedback, they were based on some ideal conditions, such as the homogeneous spatial distribution of the background environment or the existence of ideal mesoscale eddies (Bruneau et al., 2020; Lu et al., 2020), and a straight-line typhoon track (Change & Anthes, 1979; Sutyrin & Khain, 1984). In the actual typhoon-ocean interaction process, the ocean environment, typhoon track and typhoon intensity are changeable. In particular, some typhoons turn sharply during their passage, which introduces new changing factors into study the typhoon-ocean interaction process. This type of typhoon-ocean interaction process caused by typhoon motions (not uniform linear motion) is of great significance for us to fully understand typhoon-ocean interactions.

In this study, we investigate super typhoon Nida (2009), which showed three motion states: a pre-typhoon (PT) stage with a turning track, slow speed and weak intensity; a first Category 5 (FC) stage with a straight-line track, fast speed and strong intensity; and a second Category 5 (SC) stage with a sudden-turning track, extremely slow speed and strong intensity. By comparing the typhoon-ocean interaction in the different typhoon stages, the characteristics of typhoon-ocean interactions under different motions are comprehensively explained. The paper is organized as following. In section 2, we introduce the data and research methods. Section 3 presents the research results. A discussion and conclusions are provided in sections 4 and 5, respectively.

2 Data and Methods

2.1 Super typhoon Nida

Super typhoon Nida was the twenty-sixth tropical storm and fourth super typhoon of the 2009 Pacific typhoon season (Figure 1). Typhoon Nida generated in the Northwest Pacific (NWP) on 21 November 2009, and achieved typhoon intensity on 24 November. Thereafter, Nida kept moving northwest in a straight-line track and rapidly intensified until it reached the MSW speed of 155 kts on 25 November. Nida intensified by 90 kts within 24 h in the FC stage, which was much greater than definition of rapid intensification. On 28 November, Nida suddenly turned left with a maximum turning angle of 135° and weakened rapidly from 150 kts to 90 kts in the SC stage from 28 November to 30 November. After that, Nida weakened to a tropical storm on 2 December and disappeared on 3 December.

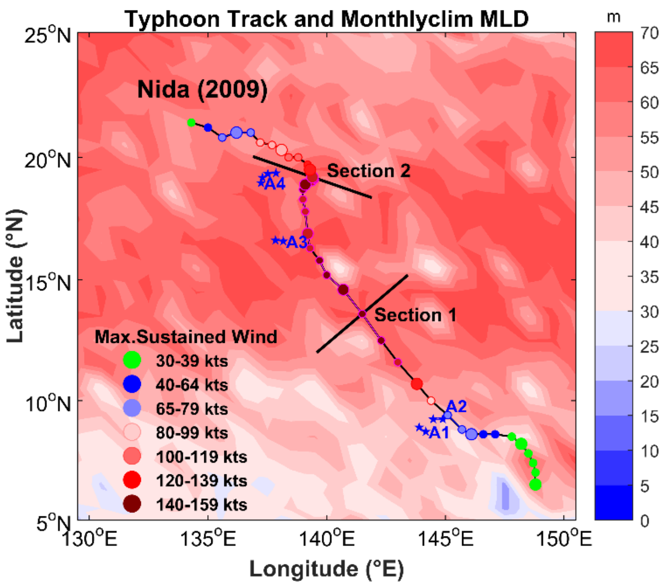

Figure 1. Best track of typhoon Nida (2009) from the JTWC. The blue stars denote the positions and trajectory of Argo floats (A1 to A4 are floats 5902121, 5901213, 5900976 and 2900401). The track line color indicates the MSW speed of the typhoon. The background pattern is the monthly

climatology MLD from November to December. The two black sections indicate the location of the strongest intensity (section 1) and maximum turning (section 2).

We defined the turning angle of a typhoon as the azimuth change of the path in the 12 hours before and 12 hours after a certain point (turn left, positive; turn right, negative). The rapid intensification of tropical cyclones was defined as a wind speed increase of 30 kts or more in a 24 h period (Wang et al., 2015).

2.2 Data

We used daily SST products with a spatial resolution of 9 km × 9 km that were integrated with microwave and infrared optimally interpolated data from Remote Sensing Systems (RSS) (www.remss.com).

The daily sea surface salinity (SSS) data with a spatial resolution of 0.25° × 0.25° were from the three-dimensional global ocean reanalysis product produced by the Copernicus Marine and Environmental Monitoring Service Global Monitoring and Forecasting Centre (http://marine.copernicus.eu/services-portfolio/access-to-products/).

The daily sea surface height anomaly (SSHA) and sea surface geostrophic velocity data with a spatial resolution of 0.25° × 0.25° were satellite altimeter data from the Ssalto/Duacs multisensor gridded delay-time altimetry product provided by Archiving, Validation and Interpretation of Satellite Oceanographic Data (AVISO) (https://www.aviso.altimetry.fr/en/data/products/) and distributed by the Copernicus Marine and Environmental Monitoring Service.

The wind vector datasets were the wind at 10 m above the sea surface from the Cross-Calibrated Multi-Platform gridded surface vector winds provided by RSS. The temporal resolution of the wind field data used is 6 h and the spatial resolution is 0.25° × 0.25°.

This study used the daily precipitation product with a spatial resolution of 0.1° × 0.1° from the Integrated Multi-satellite Retrievals for Global Precipitation

Measurement (GPM) mission.

We extracted the Argo float profiles from the real-time quality-controlled Argo database of the China Argo Real-time Data Center (http://www.argo.org.cn). In this study, four Argo floats were used (shown in Figure 1): float A1, 5901213, float A2, 5902121, float A3, 5900976 and float A4, 2900401.

The mixed layer climatology and database (Holte et al., 2017) using Argo profiles and a hybrid method (Holte & Talley, 2009) for finding the MLD have been compiled by Scripps Institution of Oceanography, UC San Diego (http://mixedlayer.ucsd.edu/).

The daily and weekly ocean color datasets with a spatial resolution of 25 km × 25 km were obtained from GlobColour (http://hermes.acri.fr/index.php?class=archive). The GlobColour merged data products are coalesced from multiple mission observations into a single data product with better spatial and temporal coverage. In addition, chl-*a* datasets obtained from the three-dimensional global ocean forecast product produced by the Copernican Marine Environmental Monitoring Service Center (http://marine.copernicus.eu/services-portfolio/access-to-products/) were used to show the weekly sea surface fields of zooplankton with a spatial resolution of 0.25° × 0.25°.

2.3 Methods

2.3.1 Ekman pumping

The upwelling (upw) caused by Ekman pumping is (Price, 1981):

$$\mathrm{upw} = \nabla \times (\tau/\rho f), \quad (1)$$

where ∇ is a gradient operator (total differential in all directions of space), called Hamilton operator, f is the Coriolis parameter, ρ is the density of seawater and τ is the wind stress vector, which can be calculated as follows:

$$\tau = \rho_{\mathrm{a}} C_{\mathrm{D}} |\mathbf{U_{10}}| \mathbf{U_{10}}, \quad (2)$$

$$C_{\mathrm{D}} = \begin{cases} (4 - 0.6|\mathbf{U_{10}}|) \times 10^{-3} & \text{for } |\mathbf{U_{10}}| < 5\ \mathrm{m/s}; \\ (0.737 + 0.0525|\mathbf{U_{10}}|) \times 10^{-3} & \text{for } 5\ \mathrm{m/s} \le |\mathbf{U_{10}}| < 25\ \mathrm{m/s}, \\ 2.05 \times 10^{-3} & \text{for } |\mathbf{U_{10}}| \ge 25\ \mathrm{m/s} \end{cases} \quad (3)$$

where ρ_a is the air density, C_{D} is the drag coefficient (Jaimes et al., 2015; Powell et al., 2003) and $\mathbf{U_{10}}$ is the 10-m wind vector.

2.3.2 Enthalpy flux and energy budget

The sensible heat flux and latent heat flux were calculated, based on the bulk aerodynamic formula under the tropical cyclone-ocean coupling condition (Cione et al., 2013; Jaimes et al., 2015; Lin et al., 2014) as follows:

$$Q_{\mathrm{S}} = C_{\mathrm{S}} V (T_{\mathrm{s}} - T_{\mathrm{a}}) \rho_{\mathrm{a}} C_{\mathrm{pa}}, \quad (4)$$

$$Q_{\mathrm{L}} = C_{\mathrm{L}} V (q_{\mathrm{s}} - q_{\mathrm{a}}) \rho_{\mathrm{a}} L_{\mathrm{va}}, \quad (5)$$

where C_{L} and C_{S} are latent and sensible heat exchange coefficients. V is the wind speed from the typhoon model in the present study (Mei et al., 2015) as follows:

$$\begin{cases} V(r) = V_{\max}\left(\frac{r}{R_{\max}}\right) & \text{for } r < R_{\max} \\ V(r) = V_{\max}(r/R_{\max})^{-n} & \text{for } r >= R_{\max} \end{cases} \quad (6)$$

where $n = 0.6$. T_{s} and T_{a} are during-typhoon SST and near-surface air temperature, respectively, and q_{s} and q_{a} are surface and air specific humidity, respectively. T_{a} and q_{a} are from the NCEP dataset. C_{pa} is the specific heat of air at constant pressure, L_{va} is the latent heat of vaporization, ρ_{a} is the air density, and q_{s} is the saturated specific humidity. The frictional heat generated by the friction between typhoon and ocean is as follows:

$$D = \rho_{\mathrm{a}} C_{\mathrm{D}} V^3, \quad (7)$$

The typhoon is regarded as a Carnot heat engine, and the heat conversion efficiency is efficiency = (SST − CTT)/SST, where CTT is the cloud top temperature. The ocean energy input into the typhoon is:

$$W = (Q_{\mathrm{S}} + Q_{\mathrm{L}} + D) \times \text{efficiency}. \quad (8)$$

The net energy input of the ocean to typhoons is $N = W - D$.

2.3.4 Grid-based maximum response method

The grid-based maximum response (GMR) method proposed by Li et al. (2020) is a new method to accurately evaluate the SST response to a typhoon by using the asynchronous SST fields. Using daily data from satellite remote sensing, this method can accurately calculate the maximum amplitude of SST cooling and the location of SST cooling centers.

2.3.5 Large-scale transport by eddy

The eddy is detected with SSHA data (Li et al., 2016). If there was a series of closed contours in the SSHA field, when the value of the outermost closed contour was greater than 6 cm, the region was defined as a warm eddy; when the outermost closed contour was less than −6 cm, the region defined was a cold eddy (Liu et al., 2017; Sun et al., 2019).

Zhang et al. (2020) evaluated the eddy effect on Kuroshio transport based on the well-known turbulent Sverdrup balance as follows:

$$S_v = \frac{1}{\beta}\int |u_{\mathrm{w}}|\ \Delta Q\ \mathrm{d}y \tag{9}$$

where β is the beta effection, u_{w} denotes the eddies' westward propagation and ΔQ denotes the potential vorticity (PV) anomaly.

3 Results

3.1 Oceanic responses in the entire area

Super typhoon Nida induced strong winds and severe rainfall during its lifespan. Figure 2a shows the cumulative Ekman pumping caused by Nida during its passage. In the PT stage and SC stage, due to the sudden turning, Nida induced a long forcing time on the upper ocean, resulting in strong accumulation of Ekman pumping. The evolution of wind stress and local Ekman pumping showed that the wind field in the study area was very weak (<10 m s^{-1}) before Nida entered (Figure S1 in SM). During the passage of typhoon Nida, strong winds prevailed with the upwelling velocity ranging from 0.1 to 0.5 m h^{-1}. Figure 2b shows the cumulative rainfall during the passage of the typhoon. The rainfall was mainly concentrated in the SC stage of the typhoon, during which the accumulated rainfall exceeded 1000 mm, and the rainfall induced by the typhoon was mainly located on the right side of the typhoon track (daily evolutions see Figure S2 in SM).

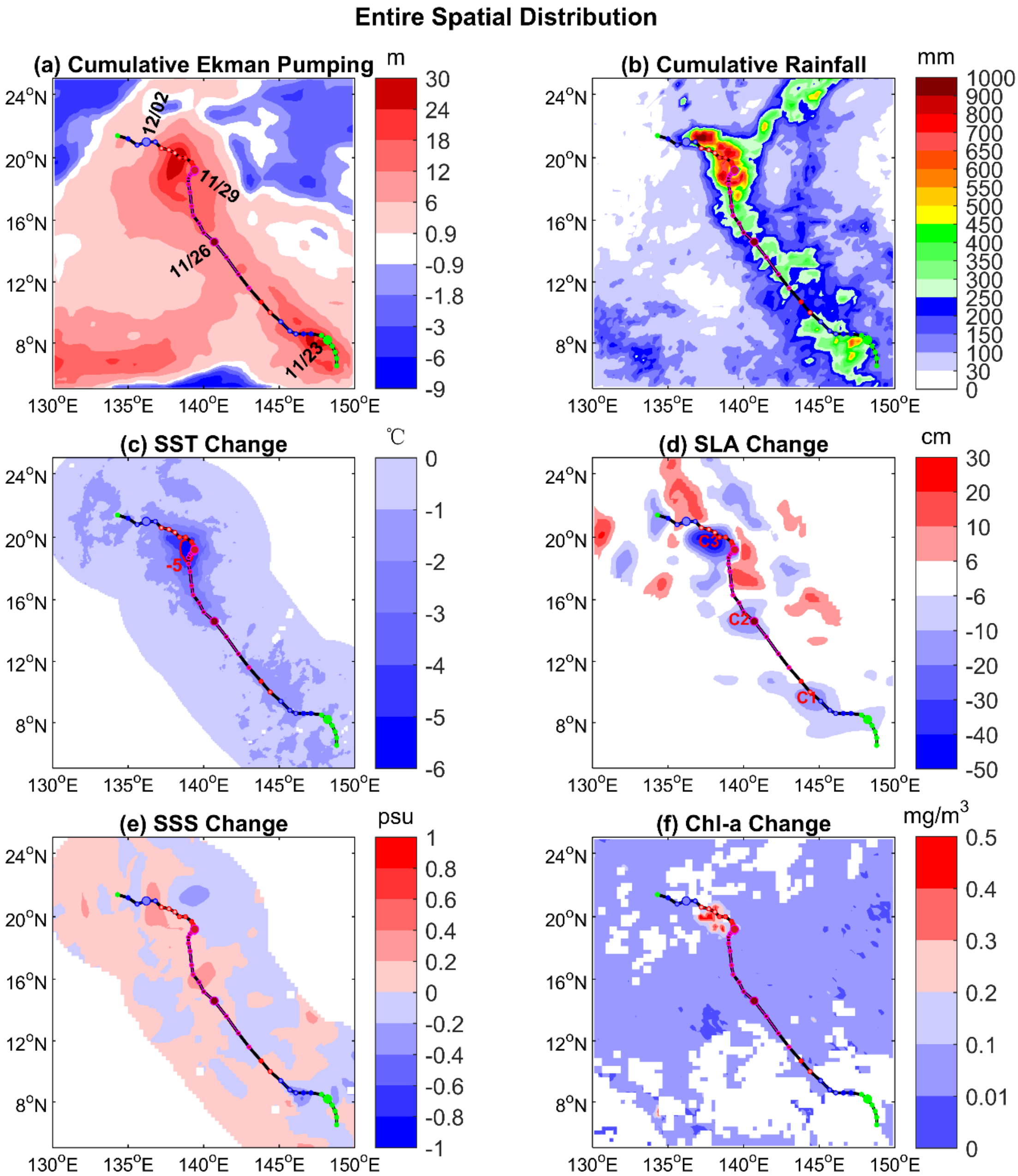

Figure 2. The entire spatial distribution of: (a) cumulative Ekman pumping; (b) cumulative rainfall; (c) SST change (the red solid line shows the 5 ℃ contour); (d) SSHA change; (e) SSS change; (f) chl-*a* change.

Figure 2c shows the SST response field calculated using the GMR method and the results show that the SST cooling mainly occurred in the SC stage of the typhoon. The SST cooling center with the maximum SST decrease of −6.68 ℃ was located about 80 km to the left of the typhoon track, and almost all of the strong cooling area greater than −5 ℃ was located on the left side of the typhoon track. The evolution of the SST fields (Figure S3 in SM) showed that the SST in the study area was dominated by warm temperatures higher than 28 ℃ before Nida entered, and SST cooling occurred during typhoon's passage. Consistent with previous studies, the cold wake was obviously lagging behind the typhoon center and the SST cooling showed an obvious right bias in the FC stage (Price, 1981; Zhang et al., 2016). In contrast, the maximum SST cooling overlapped the typhoon center and was located on the left-hand side of the track in the SC stage.

The SSHA response to Nida calculated using the GMR method was showed in Figure 2d. The results suggest three main centers along the typhoon track where the SSHAs decreased, marked as C1, C2 and C3, respectively. C3 in the SC stage was strongest and the maximum SSHA reached −60 cm. This was because of the strong typhoon intensity and long typhoon forcing time in the SC stage. In contrast, C1 and C2 in the PT stage and the FC stage were relatively weak. The evolution of the SSHAs fields (Figure S4 in SM) showed that SSHAs in the study area were mostly positive before the arrival of Nida, and SSHAs gradually decreased during typhoon's passage.

Figure 2e shows the distribution of the SSS response field calculated using the GMR method. The results show that the area where the SSS increased, with an increase of 0.6 psu, corresponded to the strong Ekman pumping area, and that the area where the SSS decreased, with a decrease of 0.6 psu, corresponded to the heavy rainfall area (daily evolutions see Figure S5 in SM). In summary, the change in SSS was mainly determined by a mechanism of competition between the asymmetric typhoon precipitation and asymmetric Ekman pumping.

Figure 2f shows the chl-*a* difference before and after Nida, indicating that the chl-*a* concentration increased by 0.5 mg m^{-3}, which was about five times that before the passage of Nida, and the chl-*a* bloom lasted for weeks after Nida passed. Compared with the SC stage, the chl-*a* concentration in the FC stage hardly changed. Furthermore, the region with the highest chl-*a* increase (Figure S6c,g in SM) corresponded to the region with the strongest SST cooling (Figure S3i,j in SM) and SSHA decrease (Figure S4i,j in SM).

Recent case studies have found that typhoons can modulate the large-scale flow, e.g., the Kuroshio Current, via cold eddy intensification (Sun et al., 2009; Wang et al., 2009; Zhang et al., 2020). In this study, we estimated the mass transport induced by the strong cold eddy caused by typhoon Nida in the sudden-turning stage. According to the eddy structure model proposed by Wang et al. (2019), the surface eddy consists of three parts: the upper surface h1, the lower surface h2 and the eddy body of height H1. The height of the cold eddy body H1 was about 300 m from Argo measurements, the upper surface h1 was about −0.3 m and the lower surface h2 was about 200 times that of the eddy amplitude h1. $\triangle Q = \left(\frac{f+\zeta}{\mathrm{H1}+\mathrm{h1}+\mathrm{h2}} - \frac{f}{\mathrm{H1}}\right) \times (\mathrm{H1} + \mathrm{h1} + \mathrm{h2})$, where ζ is the relative vorticity. The westward speed of the eddy was about 0.27 m s^{-1}. Based on equation (9), the strong cold eddy induced by Nida contributed about 0.25 Sv of mass transport to the large-scale mass transport (i.e. Kuroshio), which is about 0.6 times the total mass transport (0.4 Sv) in the South China Sea (Wang et al., 2009) and 0.4–0.6% of the total contribution to the mass transport (~40–60 Sv) by the Kuroshio. The times evolutions of mean SSHA of eddy and the transport induced by it were shown in Figure S7 in SM.

3.2 Comparison of oceanic responses in two Category 5 stages

To summarize the regularity of the typhoon–ocean interaction under different typhoon motions, we quantitatively compared the ocean responses in the two Category 5 typhoon stages in detail. Two representative locations were selected for the two stages. The first location was when Nida reached its strongest intensity with an MSW speed of 155 kts, at 18:00 UTC on 25 November in the FC stage. The second location was when Nida achieved its sharpest turning angle with a maximum turning angle of 135°, at 00:00 UTC on 29 November in the SC stage. Both locations are marked as black sections in Figure 1.

3.2.1 Direct response during typhoon passing

Figure 3 shows the time evolution of cross-track Ekman pumping, rainfall, SST, SSHAs and SSS at section 1 during 23 November to 1 December 2009. The Ekman pumping intensity at section 1 strengthened at 00:00 (UTC) on 25 November and then weakened at 00:00 (UTC) on 26 November. Meanwhile, the Ekman pumping induced by Nida was obviously stronger on the right-hand side of typhoon track in the FC stage. Figure 3b shows that the evolution of the rainfall corresponded to Ekman pumping in the time series but the rainfall appeared with a relatively leftward bias. The SST began to decrease on 24 November and appeared with a rightward bias. Figure 3d shows that the maximum SST cooling caused by Nida was about 1℃ and the maximum cooling center was located about 100 km on the right-hand side of the typhoon path. Figure 3e,f shows that the SSHA decreased from 24 November to 1 December and the decreased amplitude was about −3 cm. The SSS at section 1 changed slightly within the range from −0.02 psu to 0.02 psu (Figure 3g,h). In summary, at section 1, the Ekman pumping and rainfall were strong because Nida reached its strongest intensity of 155 kts. However, owing to the straight-line track and fast speed, the upper ocean responses, such as SST response, SSHA response and SSS response, were weak.

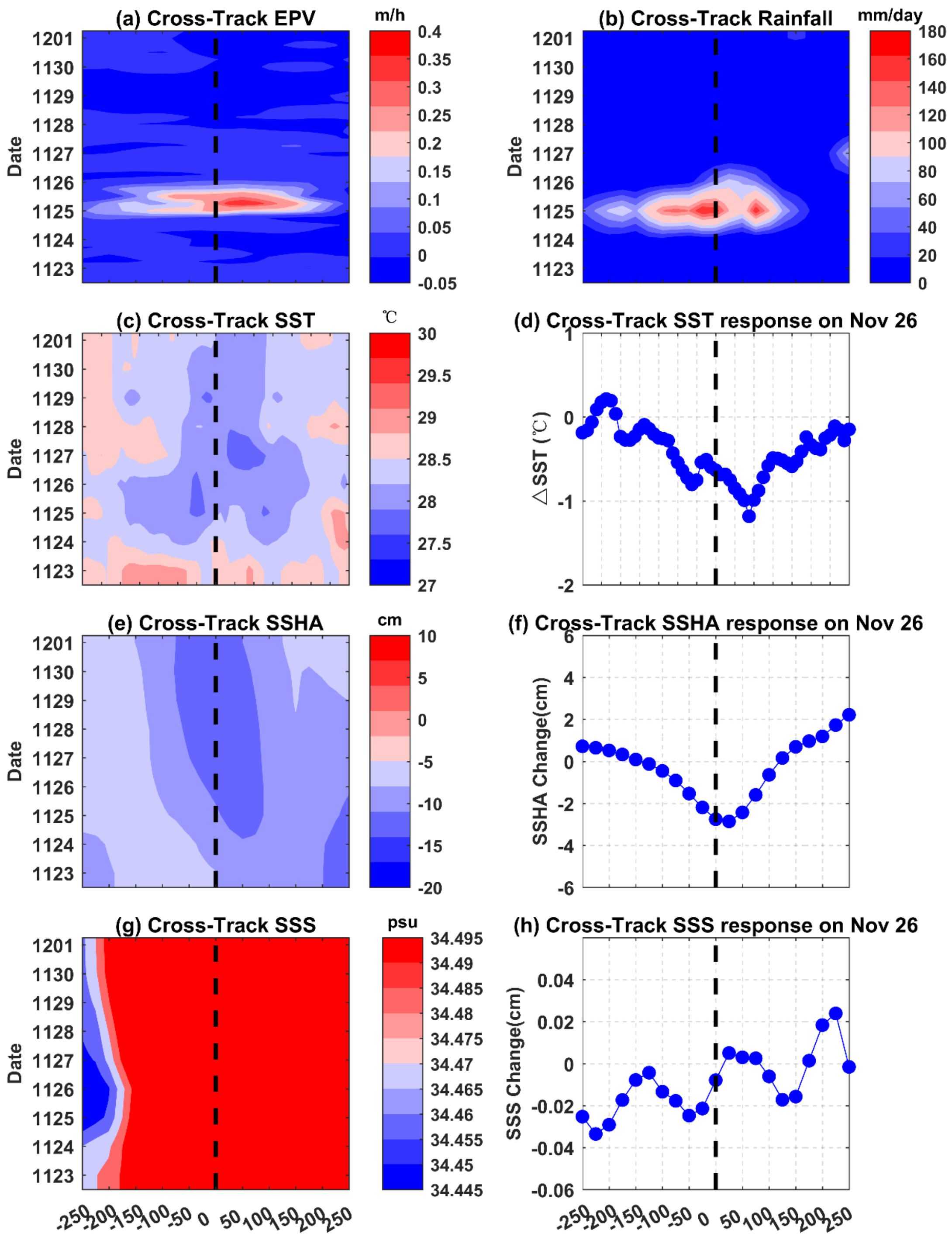

Figure 3. Time evolution of cross-track (a) cumulative Ekman pumping (shaded, m) and (b) cumulative rainfall (shaded, mm) at location 1 during the passage of typhoon Nida (23 November–1 December 2009). (c,d) Time evolution of cross-track SST (shaded, °C) and the cross-track SST response on 26 November. (e,f) Time evolution of cross-track SSHA (shaded, cm) and the cross-track SSHA response on 26 November. (g,h) Time evolution of cross-track SSS (shaded, psu) and the cross-track SSS response on 26 November.

Figure 4 shows the time evolution of the cross-track Ekman pumping, rainfall, SST, SSHAs and SSS at section 2 during 26 November to 4 December 2009. The Ekman pumping at section 2 strengthened from 27 November to 30 November and reached the maximum Ekman pumping exceeding 0.7 m h^{-1} on 29 November. It was exactly opposite to section 1, in that the Ekman pumping was obviously stronger on the left-hand side of typhoon track at section 2. Figure 4b shows that the typhoon-induced rainfall was concentrated from 27 to 30 November and the strongest rainfall exceeded 320 mm d^{-1}. The cross-track SST at section 2 began to decrease on 27 November and appeared with an obvious leftward bias (Figure 4c). The maximum SST cooling center with the maximum SST cooling exceeding 6 °C was located 80 km to the left of typhoon track (Figure 4d). Meanwhile, the SST response was relatively smaller with a maximum SST cooling of 5.42 ℃ on the right-hand side of the typhoon track. Figure 4e,f shows that the SSHAs decreased from 26 November to 4 December and the maximum SSHA decrease exceeded −30 cm. The SSS increased on the left-hand side of track but decreased on the right-hand side with the SSS response ranging from −0.05 psu to 0.05 psu at section 2 (Figure 4h). The asymmetric SSS response was dominated by asymmetric rainfall (Figure 4b). It can be clearly seen that the cross-track evolutions of SST (Figure 4c), SSHAs (Figure 4e) and SSS (Figure 4g) show a high consistency in the time series, due to the typhoon-induced Ekman pumping (Figure 4a). In summary, at section 2, the Ekman pumping and rainfall were strong and the ocean responses were notable because of the long-duration interaction and strong typhoon intensity.

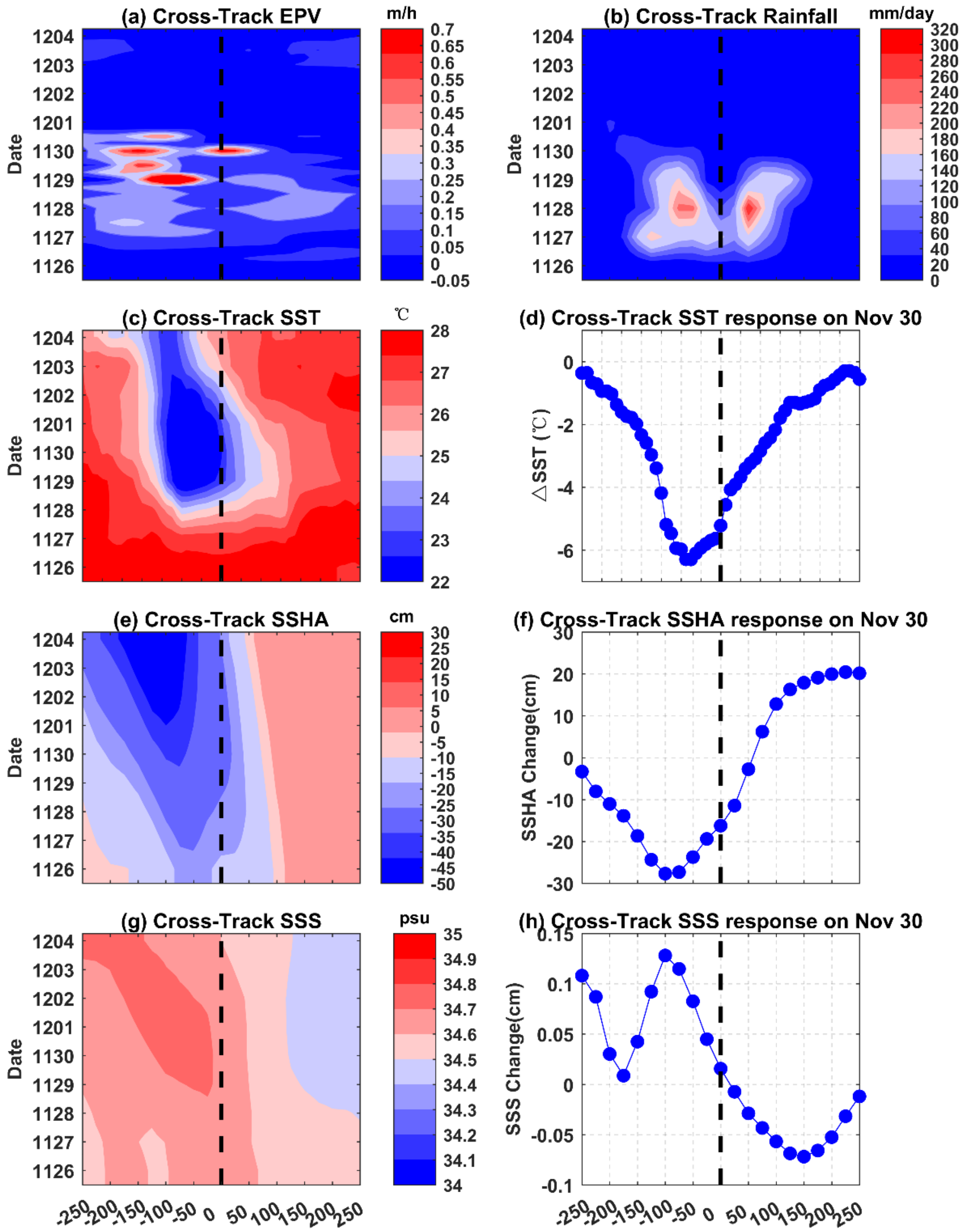

Figure 4. Time evolution of cross-track (a) cumulative Ekman pumping (shaded, m) and (b) cumulative rainfall (shaded, mm) at location 2 during the passage of typhoon Nida (30 November–4 December 2009). (c,d) Time evolution of cross-track SST (shaded, °C) and the cross-track SST response on 30 November. (e,f) Time evolution of cross-track SSHAs (shaded, cm) and the cross-track SSHA response on 30 November. (g,h) Time evolution of cross-track SSS (shaded, psu) and the cross-track SSS response on 30 November.

3.2.2 Long-memory response after typhoon passed

In addition to the direct response of the upper ocean, we have studied the long-term impact of typhoon Nida on the marine environment by comparing the marine environment two weeks after the typhoon's passage. In the FC stage, the long-memory ocean responses one week and two weeks after Nida passed showed that the SSHAs, SST and chl-*a* distribution show that the ocean responses recovered rapidly within a week (see Figure S8 in SM).

In contrast, Figure 5 shows the long-memory ocean response one week and two weeks after Nida passed in the SC stage. The SSHA response (Figure 5a,b) indicates that the strong cold eddy with an SSHA decrease of −60 cm generated by Nida in the SC stage existed and strengthened for several weeks. Figure 5c,d shows that Nida induced a maximum SST cooling exceeding 6 °C, which lasted more two weeks (Figure 5a,b). Meanwhile, the cold eddy caused a long-lasting chl-*a* bloom exceeding 0.6 mg m^{-3} and an SSS increase of 0.6 psu, as shown in Figure 5e,f and 8g,h, respectively, for several weeks after the passage of Nida, which played an important role in the upper marine ecological environment and marine material transportation. As well known, in the tropical oceans, limited nutrient concentrations in the upper ocean are not conducive to enhancing primary productivity (Lomas et al., 2012; Huang & Xu, 2018). Typhoon Nida induced the transport of richer nutrients from the subsurface to the surface layer, and together with the sufficient sunlight and strong photosynthesis after the passing of a typhoon, there was a marked increase in the surface chl-*a* concentration (five times that before the typhoon's passage). Therefore, typhoon Nida not only directly affected the upper ocean environment during its passage but also induced long-term non-negligible ocean responses by forcing the formation of cold eddy.

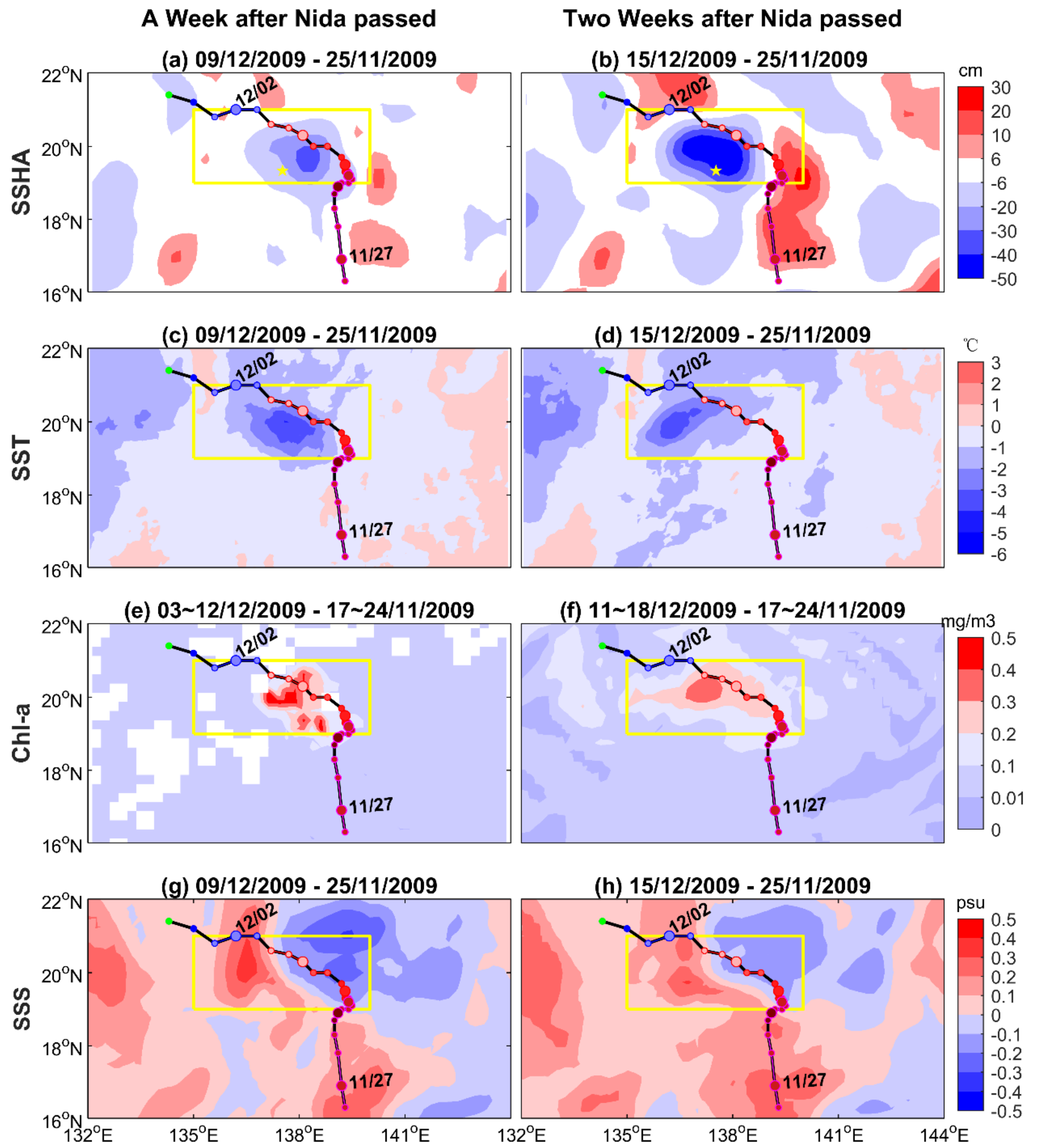

Figure 5. The sudden-turning stage. (a,b) The SSHA fields (shaded, cm) on 9 and 15 December 2009, indicating one week and two weeks after the passage of Nida, respectively. (c,d) The SST responses (shaded, cm) on 9 and 15 December 2009. (e,f) The chl-*a* and zooplankton responses (shaded, cm) several weeks after the passage of typhoon Nida. (g,h) The SSS responses (shaded, cm) on 9 and 15 December 2009. The yellow rectangle and yellow star indicate the cold eddy area and location of Argo float 2900401, respectively.

Furthermore, we quantified the average ocean responses along the typhoon track in the two Category 5 stages (Table 1). The high-latitude MLD in the SC stage was slightly deeper than the low-latitude MLD in the FC stage. The average intensity of Nida for both stages was about 120 kts. However, the turning angle and speed of Nida were quite different in the two stages. In the SC stage, the turning angle and speed was 62.48° and 0.94 m s^{-1}, respectively, which was four times and one-quarter of the turning angle of 15.68° and speed of 4.39 m s^{-1} in the FC stage. Under the conditions of a similar ocean environment and typhoon intensity, the SST response, SSHA response and chl-*a* response in the SC stage were −4.15 ℃, −10.29 cm and 0.12 mg m^{-3}, respectively, which were three times, two times and four times that in the FC stage. In summary, owing to the difference in turning angle and speed, the upper ocean responses during the SC stage are about three times more than that in the FC stage.

Table 1.

The quantitative impact factors and biophysical responses in the two Category 5 stages.

	The FC stage	The SC stage
Monthlyclim MLD (m)	52.80	61.91 (↑)
MSW speed (kts)	120.77	120.00 (=)
Turning angle (degree)	15.68	62.48 (↑)
Translation speed (m/s)	4.39	0.94 (↓)
Rainfall (mm/day)	264.58	601.02 (↑)
SST response (℃)	-1.44	-4.15 (↑)
SSHA response (cm)	-5.00	-10.29 (↑)
SSS response (psu)	0.06	0.00 (↓)
Chl-a response (mg/m^3)	0.03	0.12 (↑)

Note. The MLD, rainfall, SST, SSHA, SSS and chl-*a* were averaged along the typhoon in the two stages.

3.2.3 Subsurface response

To investigate the subsurface response, we analyzed vertical profiles measured by

Argo floats before and after typhoon Nida (Figure 6). Typhoon Nida affected floats 5901213 and 5902121 on 24 November. At this time, Nida moved fast and its intensity was weak with an MSW speed of 65 kts. As shown in Figure 6a, the thickness of the mixed layer showed no obvious change after Nida passed. Nida affected float 5900976 from 26 to 27 November after it reached the maximum intensity, increasing MLD by 35 m (Figure 6c). The float 2900401 was located at the sudden-turning track and affected by Nida from 28 November to 1 December. During this stage, MLD increased by 50 m (Figure 6e). At all three locations, the subsurface temperature responses showed a three-layer vertical structure of decreasing–increasing–decreasing (Figure 6b,d,f). In addition, Figure 6g,h shows the time evolution of temperature and salinity profiles measured by Argo float 2900401. First, Nida induced strong vertical mixing that not only cooled the surface but also heated the subsurface, which is the so-called ‘heat pump’ effect of the typhoon. In the following, the cyclonic stress of the typhoon caused a strong uplift of the ocean thermocline, which acted as a ‘cold suction’ to the upper ocean. Therefore, the upper ocean response to typhoon Nida consisted of two consequent processes: strong vertical mixing and long-lasting upwelling.

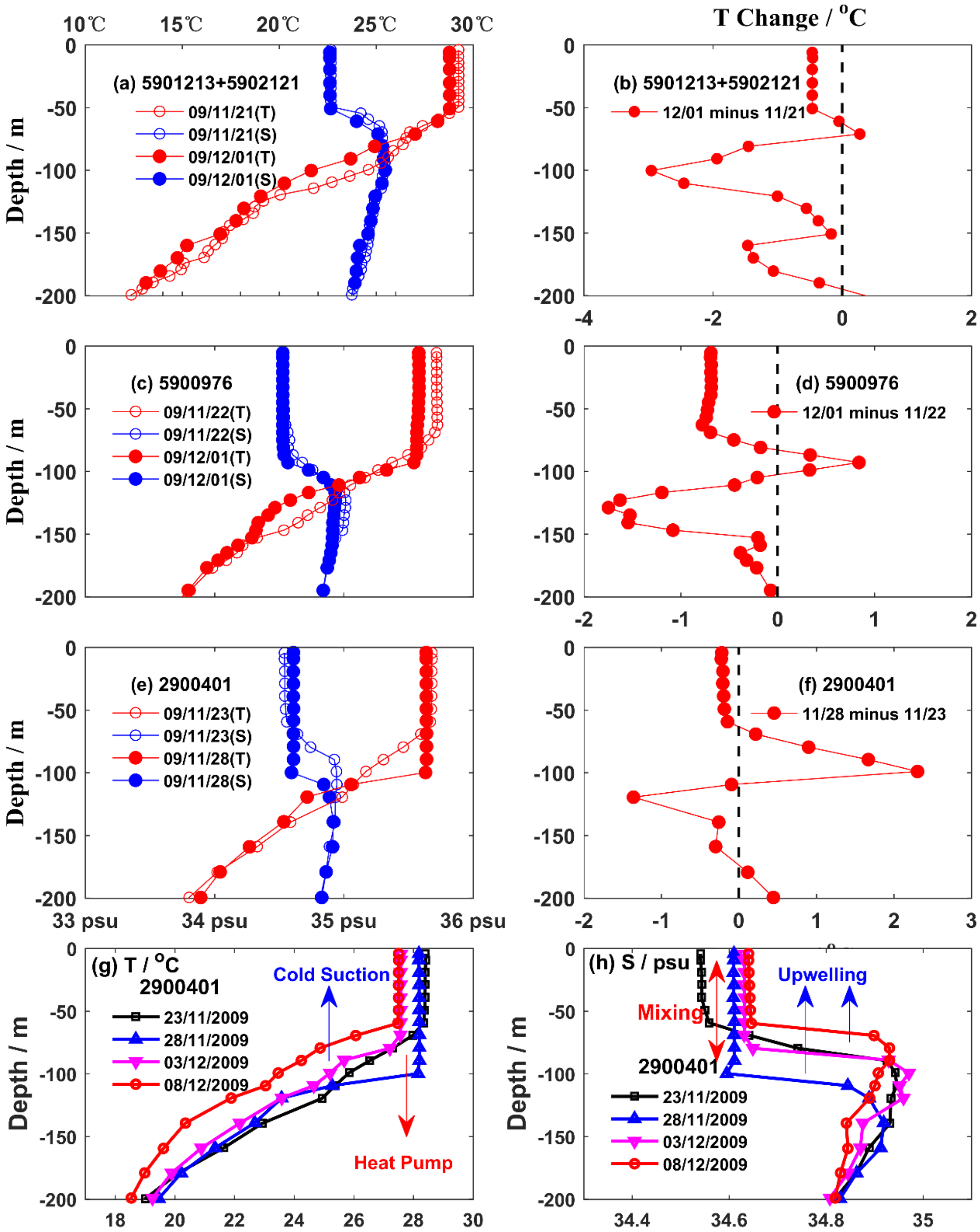

Figure 6. Temperature and salinity profiles, and temperature differences between the post-storm and pre-storm measured by Argo floats 5901213 and 5902121 (a,b), 5900976 (b,c) and 2900401 (e,f). (g,h) Time evolution of temperature and salinity profiles measured by Argo float 2900401 before and after Nida.

3.3 Upper ocean feedback to typhoon Nida

To investigate the negative feedback of the cold wake on the typhoon intensity, Figure 7 shows the evolution of Nida's inner-core cold wake and inner-core enthalpy flux (sensible heat flux and latent heat flux) in the two Category 5 stages. According to previous studies (Cione & Uhlhorn, 2003; Cione, 2015), we defined the typhoon inner core as the distance within a radius of 100 km from the typhoon center, indicated by the black solid circle in Figure 7. When Nida moved in a straight line in the FC stage, the cold wake induced by Nida lagged far behind the inner-core area because of Nida's fast speed (Figure 7a,b). Figure 7e,f indicates that the air-sea enthalpy flux supplied from the ocean to Nida was considerable, especially on 26 November, with the maximum enthalpy flux exceeding 1000 W m^{-2}. Therefore, Nida rapidly intensified in the FC stage. However, in the SC stage, the inner-core SST cooling was notable because the local cold wake no longer lagged behind the typhoon center but completely overlapped the typhoon's inner core due to the sudden-turning track of the typhoon (Figure 7c,d). The strong inner-core SST cooling resulted in a sharp decrease of the enthalpy fluxes at the sea-air interface and the inner-core enthalpy flux decreased sharply from 681.92 W m^{-2} on 26 November to −101.15 W m^{-2} on 30 November, especially on the left-hand side of track (Figure 7g,h). Furthermore, the sharp decrease of the inner-core enthalpy fluxes caused the energy supply from the ocean to typhoon to cease, rapidly weakening the intensity of typhoon Nida from Category 5 to Category 2.

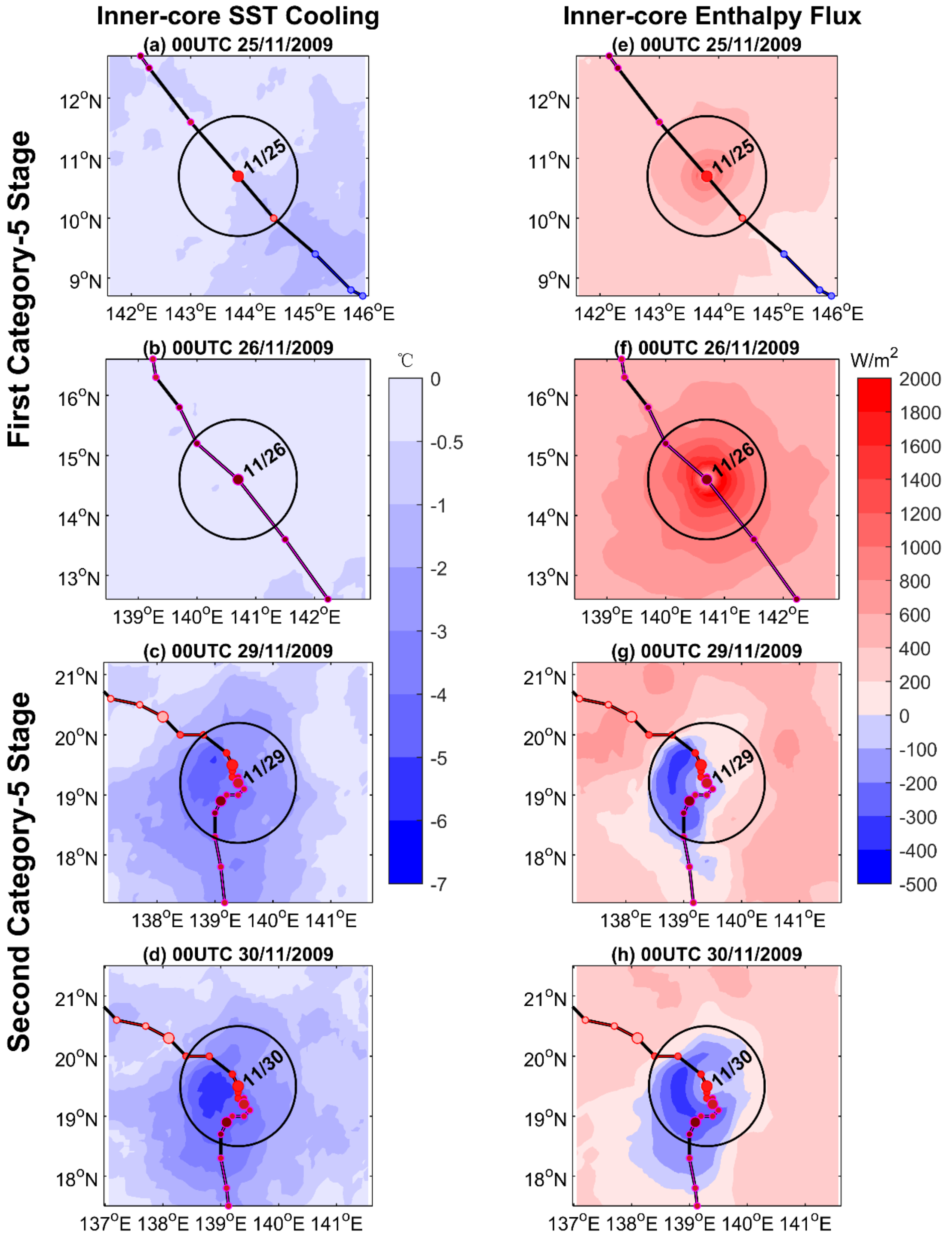

Figure 7. Evolution of the inner-core SST cooling (shaded, ℃) and inner-core enthalpy flux (shaded, W m^{-2}) in the FC stage and SC stage. The black solid circle line represents the radius of 100 km of typhoon, indicating the inner core of the typhoon.

Figure 8 shows the change of the typhoon turning angle (a), translation speed (b), inner-core SST cooling and local △SST wake (c), enthalpy flux and frictional flux (d), input power and net power (e) during the lifecycle of typhoon Nida. Meanwhile, the feedback factor F_{sst} and the center pressure depression (ΔPc) of Nida in Schade & Emanuel (1999)'s research were calculated in Figure 8f and g. In the PT stage (22–24 November), Nida turned left (Figure 8a) and moved at a speed of about 2 m s^{-1} (Figure 8b). The local cold wake, inner-core SST cooling caused by Nida (Figure 8c), the energy input from ocean into typhoon (Figure 8d,e) were very weak because the sea surface winds induced by Nida were weak. The feedback factor F_{sst} was relative strong because Nida moved slowly along the turning track (Figure 8f). Therefore, due to weak energy from ocean and strong F_{sst}, Nida's intensity strengthened slowly (Figure 8g) in the PT stage.

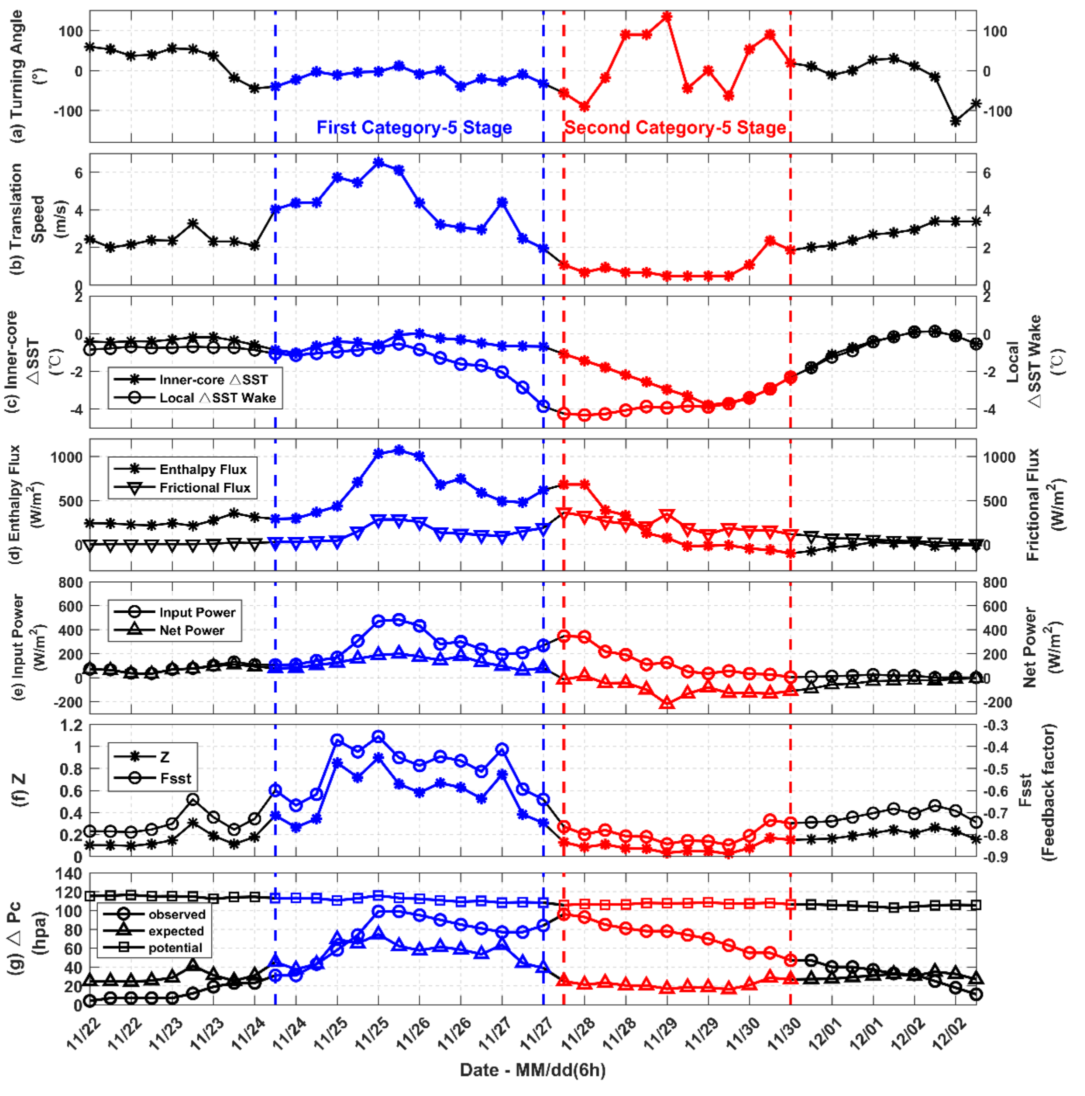

Figure 8. (a) The turning angle (°), (b) transform speed (m s^{-1}), (c) inner-core SST cooling and local △SST wake (°C), (d) enthalpy flux and frictional flux (W m^{-2}), (e) input power and net power (W m^{-2}), (f) the feedback factor F_{sst} and reference value Z in Schade & Emanuel (1999), (g) Observed, expected and potential pressure depression in the eye of typhoon Nida during its passage. The blue and red segments indicate the straight-line stage and the sudden-turning stage of typhoon Nida.

On 24 November, Nida strengthened to typhoon intensity and evolved into the FC stage. In the FC stage, the typhoon track of Nida was close to a straight line (Figure 8a) and the maximum translation speed reached 6.36 m s^{-1} (Figure 8b), as shown by the blue line segment in Figure 8. Because Nida moved along a straight-line track and the speed was fast, the local cold wake caused by the typhoon was very weak (Figure 8c). As the speed gradually slowed to 4 m s^{-1}, the typhoon-induced local cold wake gradually strengthened to −3 °C. Cione & Uhlhorn (2003) showed that it took 23 h for the background temperature to change into a cold wake. Assuming that the radius of the cold wake is 100 km, if the inner-core area is to feel the cold wake, the speed of the typhoon should be slower than 2 m s^{-1}. Therefore, when the speed of the typhoon slowed to 4 m s^{-1}, although the typhoon-induced local cold wake gradually strengthened, the inner-core SST cooling was still weak. The environment in the inner-core area still provided favorable conditions for the development of the typhoon. In this stage, the enthalpy flux supplied by the ocean to the typhoon increased to 1000 W m^{-2} (Figure 8d), and the corresponding input power (and net power) from the tropical ocean to Nida increased to 500 (200) W m^{-2} (Figure 8e). The feedback factor F_{sst} of Nida in this stage was very weak with the value above -0.4 (Figure 8f). Therefore, because of the strong energy from ocean and weak F_{sst}, Nida rapidly intensified to a Category 5 typhoon with a ΔPc of 99 hpa and MSW speed of 155 kts, and the intensification rate is about three times the definition of rapid intensification in the previous studies (Figure 8g).

On 27 November, Nida suddenly turned left and evolved into the SC stage. In the SC stage, the maximum turning angle of Nida reached 135° (Figure 8a), and the typhoon moved very slowly, about 1 m s^{-1} (Figure 8b), as shown by the red line segment in the Figure 8. Owing to the sharp turning and extremely slow speed, the typhoon caused a strong cold wake over −4 ℃ (Figure 8c). At the same time, the sharp turning and slow speed resulted in the typhoon center revisiting and staying over the cold wake, and the inner-core SST began to drop rapidly to −4 ℃. The decrease of the inner-core SST resulted in a rapid decrease in the enthalpy flux supplied by the ocean to Nida (Figure 8d), and the corresponding input power (and net power) decreased to 50 (−200) W m^{-2} (Figure 8e). The feedback factor F_{sst} strengthened rapidly to -0.85 because of Nida's extremely slow translation speed along sudden-turning track (Figure 8f). As shown in Figure 8g, Nida weakened from Category 5 with the ΔPc of 96 hpa to Category 2 with the ΔPc of 55 hpa before and after the SC stage. In summary, owing to the different motions of typhoon Nida in the different stages, the ocean's responses and feedbacks to the typhoon were quite different in the different stages.

4 Discussion

Although there were negative feedbacks on Typhoon Nida's intensity, the statistical regression of feedback F_{sst} (Schade & Emanuel, 1999) was several times larger than the measured intensity change, as shown in Figure. 8. The overestimation of the feedback F_{sst} might result in overestimation of negative feedback time. The feedback F_{sst} was obtained from statistical regression of steady-state intensity of the hurricane in model simulations. According to the numerical simulations (Schade & Emanuel, 1999; Ma et al., 2020), it takes storm more than 2-3 days to settle into a statistically steady state in coupled models. This time in general is much longer than the interaction time between typhoon and ocean cold wake. Thus, the negative feedbacks were too weak to be noted in observations.

Although the negative feedback generally were too weak to kill typhoon, it may suppress typhoon's intensity as in Figure 8g. Typhoon Nida is not an isolated case. For typhoon Hagibis in 2007 (Sun et al., 2010), and typhoon Prapiroon in 2012 (Li et al., 2014), the curved typhoon tracks caused them to undergo a similar process: generation and revisiting of a cold eddy and the negative feedback process suppressed their intensity to below Category 1.

Besides, we consider which parameter might be dominate, although the negative feedback factor z includes many parameters such as SST, ocean mixed-layer depth (MLD), ocean stratification, typhoon translation speed, typhoon size, latitude, and so on (Schade & Emanuel, 1999). This can be seen from Figure 8b and f, both curves have similar variation, their correlation is 0.847. This implies that the dominate parameter of negative feedback is translation speed in case of Typhoon Nida.

The sharp sudden-turning track is an effect way of slowing translation speed. When the typhoon moves along a straight-line track, the typhoon needs to move at a very slow speed (<2 m s^{-1}) for a significant negative feedback, which is restricted by the radius of typhoon core and cold wake. According to statistics, in the North Atlantic, for about 15% of the duration of a typhoon, the speed is below 2 m s^{-1}, and only 3% of the time is below 1 m s^{-1} (Yablonsky & Ginis, 2009); in the Pacific Ocean, the proportion of time below 2 m s^{-1} may be as low as 10% (Lin et al., 2014). According to our statistics, only 6% of typhoons in the NWP moved slower than 2 m s^{-1} in the past 40 years from 1981 to 2018, while the proportion below 1 m s^{-1} was as low as 1% (Figure 9a). Therefore, for a typhoon that moves in a straight line at a typical speed (4–6 m s^{-1}), even if there is a decrease in SST, negative feedback hardly exists (Change & Anthes, 1979). However, when a typhoon moves along a sudden-turning track, the equivalent speed of the typhoon is greatly reduced, which is equivalent to the typhoon staying in a specific area for a long time, increasing the probability of negative feedback. According angle statistics (Figure 9b), more than 60% of typhoons are close to straight (amplitude of turning angle <20°), and due to the influence of the NWP subtropical high pressure and large-scale circulation, more than 60% of typhoons turn right. Note in particular, typhoons with a turning angle greater than 50° are about 10%, which can increase the probability that typhoons revisit the cold wakes, thus enhancing the negative feedback effect that is difficult to trigger.

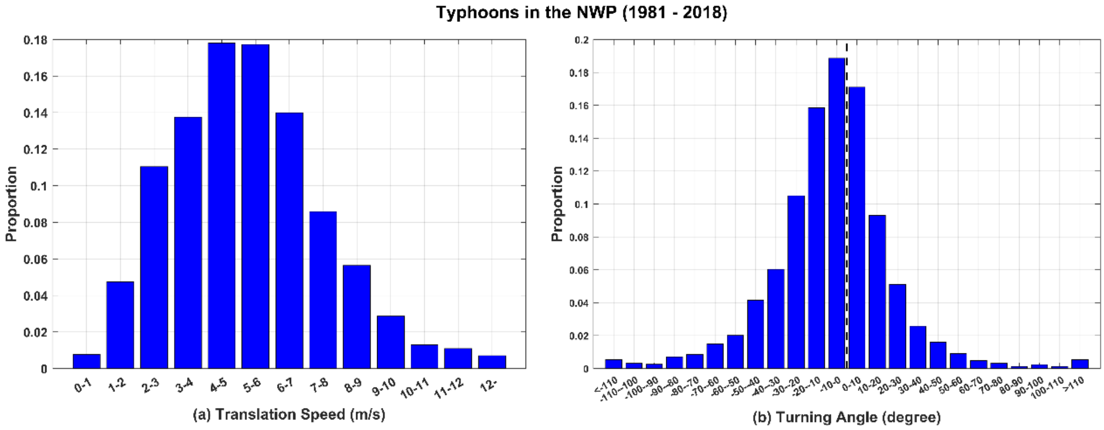

Figure 9. The distribution of typhoon (a) translation speed and (b) turning angle in the NWP during recent 40 years from 1981 to 2018.

5 Conclusions

Super typhoon Nida generated in the NWP in 2009 and consisted of a pre-typhoon stage and two Category 5 stages. In the pre-typhoon stage (PT stage), Nida intensified from a tropical depression to a Category 1 typhoon. In the first Category 5 stage (FC stage), Nida moved quickly along a straight-line track and rapidly intensified from Category 1 to Category 5. In the second Category 5 stage (SC stage), Nida moved slowly along a sharp-left sudden-turning track and weakened from Category 5 to Category 2. Hence, Nida is a special super typhoon case that included three typical stages at the same time and the research on the interaction between Nida and the ocean could be used as a template to study the typhoon-ocean interaction process. Summarizing the regularity of typhoon-ocean interaction under different typhoon motions can provide a comprehensive and in-depth understanding of the typhoon–ocean interaction process. Based on this study, a schematic of the interaction between the typhoon and the ocean, including the three stages (the PT stage, the FC stage and the SC stage), is shown in Figure 10.

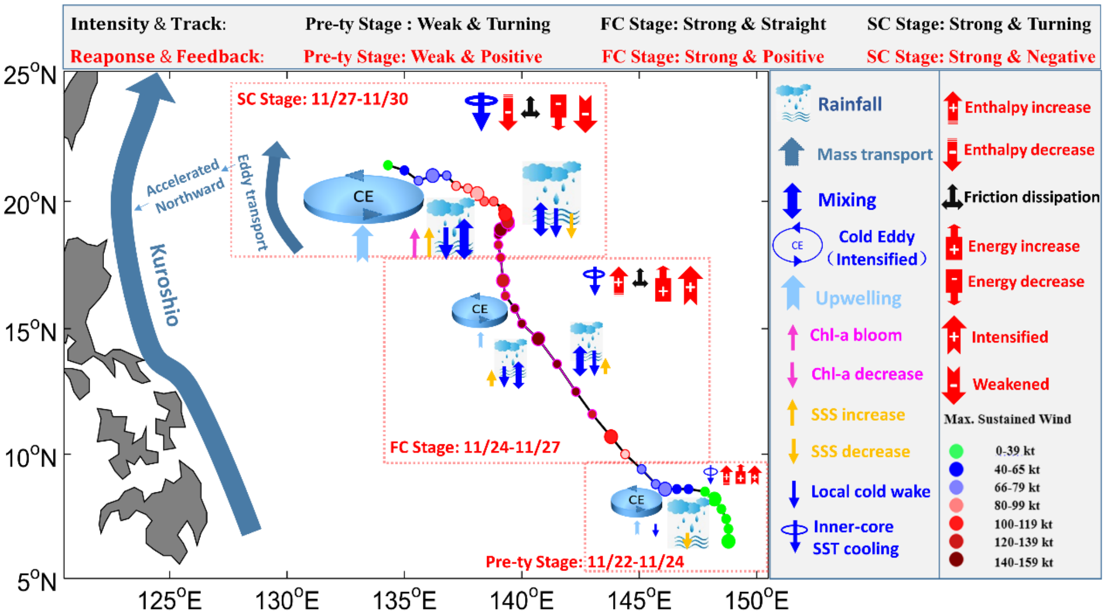

Figure 10. Schematic of the interaction between super typhoon Nida and the ocean environment.

In the PT stage (22–24 November), Nida turned left with a slow speed close to 2 m s^{-1} and intensified from a tropical depression to a category 1 typhoon with an MSW speed of 65 kts. Owing to the weak intensity in this stage, the typhoon wind was not strong enough to alter the pre-existing ocean environment, and thus could not induce intense vertical mixing and strong SST cooling. The inner-core SST cooling was relatively weak because of the weak local SST cooling; thus the ocean supplied a positive enthalpy flux and net input power provided favorable conditions for the intensification and development of typhoon Nida. Thus, in the weak intensity stage after Nida generated, Nida would have rapidly intensified regardless of the typhoon's track and translation speed.

In the FC stage (24–27 November), Nida moved fast and on a straight northwest line and the intensity strengthened rapidly from 65 kts to 155 kts. The strong wind induced strong vertical mixing and Ekman pumping. However, Nida caused only weak SST cooling because of the straight-line track and fast speed. As it slowed below

4 m s^{-1}, the ocean response gradually strengthened. During the whole stage, Nida induced an average SST cooling of −1.44 °C, an SSHA response of −5.00 cm and a chl-*a* response of 0.03 mg m^{-3}. Meanwhile, Nida's inner-core SST cooling was weaker than −0.5 °C due to the fast speed along a straight-line track. Consequently, the enthalpy flux supplied from the ocean to the typhoon remained at a high level with a maximum flux exceeding 1000 W m^{-2}, which intensified Nida from Category 1 to Category 5.

In the SC stage (27–30 November), Nida suddenly turned left with a maximum turning angle of 135° and its translation speed was slower than 1 m s^{-1}. Owing to the strong intensity and long-duration forcing in the SC stage, Nida induced strong ocean responses on the left-hand side of the track and the average SST response, SSHA response and chl-*a* response was −4.15 °C, −10.29 cm and 0.12 mg m^{-3}, respectively, which was three times, two times and four times more than that in the FC stage. Nida also induced a strong cold eddy (SSHA < −60 cm, maximum SST cooling < −6.68 °C), which caused a chl-*a* bloom exceeding 0.6 mg m^{-3} (more than five times) that lasted for weeks, which had significant impacts on the upper ocean ecological environment. This strong cold eddy also potentially enhanced the Kuroshio Current as it approached the current, accelerating it by about 0.25 Sv. The strong oceanic responses in turn induced a negative feedback to Nida's intensity. The average inner-core SST cooling of Nida reached −4°C, which resulted in a dramatic decrease in the sensible and latent heat fluxes at the sea–air interface from 681.92 W m^{-2} to −101.15 W m^{-2}. Then, the sharp decrease in the enthalpy flux terminated the net energy supply from the ocean to the typhoon and further continually weakened the intensity of Nida from 150 kts (Category 5) to 90 kts (Category 2) within three days.

It is concluded that the ocean response is weak when the typhoon intensity is weak or the typhoon speed is fast (>6 m s^{-1}) along a straight-line track. The ocean response is much stronger when the typhoon intensity is stronger and the speed is slower (~4 m s^{-1}). However, the ocean negative feedback to the typhoon intensity needs stricter conditions. According to the present case, the ocean negative feedback requires that the typhoon moves at a slow speed (<2 m s^{-1}), otherwise, the inner core of the typhoon cannot feel the local SST cooling, and the negative feedback might be negligible. In addition, the ocean negative feedback may weaken and/or suppress the typhoon intensity. However, such negative feedback may not be as strong as that suggested in previous studies. This might be due to the fact that SST is not the only factor affecting the typhoon intensity. Other factors (including, e.g., atmospheric conditions, the interaction between typhoon and land) may also have roles.

Acknowledgements

This work was supported by the National Foundation of Natural Science of China (No. 41876013) and the National Program on Global Change and Air–Sea Interaction (GASI-IPOVAI-04). We thank Remote Sensing Systems for the SST and sea surface wind data (http://www.remss.com/), GlobColour for chl-a product (http://hermes.acri.fr/index.php?class=archive), National Aeronautics and Space Administration's Precipitation Processing System for the Integrated Multi-satellite Retrievals for GPM final precipitation product (https://pmm.nasa.gov/data-access/downloads/gpm), Copernicus Marine and Environmental Monitoring Service Center for the SSS and zooplankton data (http://marine.copernicus.eu/services-portfolio/access-to-products/), Archiving, Validation and Interpretation of Satellite Oceanographic for the SSHA and Geostrophic Velocity data (https://www.aviso.altimetry.fr/en/data/products/), China Argo Real-time Data Center for Argo measurements (http://www.argo.org.cn), and Scripps Institution of Oceanography, UC San Diego for MLD data (http://mixedlayer.ucsd.edu/).

The authors declare that they have no known competing financial interests or personal relationships that could have appeared to influence the work reported in this

paper.

References

Bruneau, N., Wang, S., & Toumi, R. (2020). Long memory impact of ocean mesoscale temperature anomalies on tropical cyclone size. *Geophysical Research Letters*, *47*(6), e2019GL086165. doi: 10.1029/2019GL086165

Chacko, N. (2018). Insights into the haline variability induced by cyclone Vardah in the Bay of Bengal using SMAP salinity observations. *Remote Sensing Letters*, *9*(12), 1205-1213. doi: 10.1080/2150704X.2018.1519271

Change, S. W., & Anthes, R. A. (1979). The mutual response of the tropical cyclone and the ocean. *Journal of Physical Oceanography*, *9*(1), 128-135. doi: 10.1175/1520-0485(1979)0092.0.CO;2

Cione, J. J., & Uhlhorn, E. W. (2003). Sea surface temperature variability in hurricanes: implications with respect to intensity change. *Monthly Weather Review*, *131*(8), 1783-1796. doi: 10.1175//2562.1

Cione, J. J., Kalina, E. A., Zhang, J. A., & Uhlhorn, E. W. (2013). Observations of air–sea interaction and intensity change in hurricanes. *Monthly Weather Review*, *141*(7), 2368-2382. doi: 10.1175/MWR-D-12-00070.1

Cione, J. J. (2015). The relative roles of the ocean and atmosphere as revealed by buoy air–sea observations in hurricanes. *Monthly Weather Review*, *143*(3), 904-913. doi: 10.1175/MWR-D-13-00380.1

Emanuel, K. A. (1986). An air-sea interaction theory for tropical cyclones. Part I: steady-state maintenance. *Journal of the Atmospheric Sciences*, *43*(6), 585-604. doi: 10.1175/1520-0469(1986)043<0585:AASITF>2.0.CO;2

Emanuel, K. A. (1999). Thermodynamic control of hurricane intensity. *Nature*, *401*(6754), 665-669. doi: 10.1038/44326

Emanuel, K. A. (2018). 100 years of progress in tropical cyclone research. *Meteorological Monographs*, *59*(15), 1-68. doi: 10.1175/AMSMONOGRAPHS-D-18-0016.1

Holte, J., & Talley, L. (2009). A new algorithm for finding mixed layer depths with applications to Argo data and subantarctic mode water formation. *Journal of Atmospheric and Oceanic Technology*, *26*(9), 1920-1939. doi: 10.1175/2009JTECHO543.1

Holte, J., Talley, L. D., Gilson, J., & Roemmich, D. (2017). An Argo mixed layer climatology and database. *Geophysical Research Letters*, *44*(11), 5618-5626. doi: 10.1002/201GL073426

Huang, J., & Xu, F. (2018). Observational Evidence of Subsurface Chlorophyll Response to Mesoscale Eddies in the North Pacific. *Geophysical Research Letters*, *45*(16), 8462-8470. doi: 10.1029/2018GL078408

Jaimes, B., Shay, L. K., & Uhlhorn, E. W. (2015). Enthalpy and momentum fluxes during hurricane Earl relative to underlying ocean features. *Monthly Weather Review*, *143*(1), 111-131. doi: 10.1175/MWR-D-13-00277.1

Li, J., Sun, L., Yang, Y., & Cheng, H. (2020). Accurate evaluation of sea surface temperature cooling induced by typhoons based on satellite remote sensing observations. *Water*, *12*(5), 1413. doi: 10.3390/w12051413

Li, Q.-Y., Sun, L., & Lin, S.-F. (2016). GEM: a dynamic tracking model for mesoscale eddies in the ocean. *Ocean Science*, *12*(6), 1249-1267. doi: 10.5194/os-12-1249-2016

Li, Y.-X., Yang, Y.-J., Sun, L., & Fu, Y.-F. (2014). The upper ocean environment responses to typhoon Prapiroon (2012). *Proceedings of SPIE*, *9261*, 92610U. doi: 10.1117/12.2069263

Lin, I.-I., Liu, W. T., Wu, C.-C., Wong, G. T. F., Hu, C., Chen, Z., Liang, W.-D., Yang, Y. & Liu, K.-K. (2003). New evidence for enhanced ocean primary production triggered by tropical cyclone. *Geophysical Research Letters*, *30*(13), 1718. doi:10.1029/2003GL017141

Lin, I.-I., Pun, I.-F., & Wu, C.-C. (2009). Upper ocean thermal structure and the western north pacific category-5 typhoons. Part II: dependence on translation speed. *Monthly Weather Review*, *146*(11), 3744–3757. doi: 10.1175/2009MWR2713.1

Lin, I.-I., Pun, I.-F., & Lien, C.-C. (2014). “Category-6” supertyphoon Haiyan in global warming hiatus: Contribution from subsurface ocean warming. *Geophysical Research Letters*, *41*(23), 8547-8553. doi:10.1002/ 2014GL061281

Liu, S.-S., Sun, L., Wu, Q., & Yang, Y.-J. (2017). The responses of cyclonic and anticyclonic eddies to typhoon forcing: the vertical temperature-salinity structure changes associated with the horizontal convergence/divergence. *Journal of Geophysical Research: Oceans*, *122*(6), 4974-4989. doi: 10.1002/2017JC012814

Liu, S., Li, J., Sun, L., Wang, G., Tang, D., Huang, P., Yan, H., Gao, S., Liu, C., Gao, Z., et al. (2020). Basin-wide responses of the South China Sea environment to Super Typhoon Mangkhut (2018). *Science of the Total Environment*, *731*, 139093. doi:10.1016/j.scitotenv.2020.139093

Liu, Y., Tang, D., & Evgeny, M. (2019). Chlorophyll concentration response to the typhoon wind-pump induced upper ocean processes considering air–sea heat exchange. *Remote Sensing*, *11*(15), 1825. doi: 10.3390/rs11151825

Lomas, M. W., Moran, S. B., Casey, J. R., Bell, D. W., Tiahlo, M., Whitefield, J., Kelly, R. P., Mathis, J. T., & Cokelet, E. D. (2012). Spatial and seasonal variability of primary production on the Eastern Bering Sea shelf. *Deep-Sea Research II*, *65-70*(SI), 126–140. doi: 10.1016/j.dsr2.2012.02.010

Lu, Z., Wang, G., & Shang, X. (2020). Strength and spatial structure of the perturbation induced by a tropical cyclone to the underlying eddies. *Journal of Geophysical Research: Oceans*, *125*(5), e2020JC016097. doi: 10.1029/2020JC016097

Ma, Z., Fei, J., Huang, X., Cheng, X., & Liu, L. (2020). A study of the interaction between Typhoon Francisco (2013) and a cold-core eddy. Part II: boundary layer structures. *Journal of the Atmospheric Sciences*, *77*(8), 2865-2883. doi: 10.1175/jas-d-19-0339.1

Mei, W., Lien, C.-C., Lin, I.-I., & Xie, S.-P. (2015). Tropical cyclone–induced ocean response: a comparative study of the South China Sea and tropical Northwest Pacific. *Journal of Climate*, *28*(15), 5952-5968. doi: 10.1175/JCLI-D-14-00651.1

Powell, M. D., Vickery, P. J., & Reinhold, T. A. (2003). Reduced drag coefficient for high wind speeds in tropical cyclones. *Nature*, *422*(6929), 279-283. doi: 10.1038/nature01481

Price, J. F. (1981). Upper ocean response to a hurricane. *Journal of Physical Oceanography*, *11*(2), 153-175. doi: 10.1175/1520-0485(1981)011

Schade, L. R., & Emanuel, K. A. (1999). The ocean's effect on the intensity of tropical cyclones results from a simple coupled atmosphere-ocean model. *Journal of the Atmospheric Sciences*, *56*(4), 642-651. doi: 10.1175/1520-0469(1999)0562.0.CO;2

Shang, S., Li, L., Sun, F., Wu, J., Hu, C., Chen, D., Ning, X., Qiu, Y., Zhang, C., & Shang, S. (2008). Changes of temperature and bio-optical properties in the South China Sea in response to typhoon Lingling, 2001. *Geophysical Research Letters, 35*(10), L10602. doi:10.1029/ 2008GL033502

Stramma, L., Cornillon, P., & Price, J. F. (1986). Satellite observations of sea surface cooling by hurricanes. *Journal of Geophysical Research: Oceans*, *91*(C4), 5031-5035. doi: 10.1029/JC091iC04p05031

Sun, L., Yang, Y.-J., & Fu, Y.-F. (2009). Impacts of Typhoons on the Kuroshio Large Meander Observation Evidences. *Atmospheric and Oceanic Science Letters*, *2*(1), 45-50. doi:10.1080/16742834.2009.11446772

Sun, L., Yang, Y.-J., Xian, T., Lu, Z., & Fu, Y.-F. (2010). Strong enhancement of chlorophyll a concentration by a weak typhoon. *Marine Ecology Progress Series*, *404*, 39-50. doi: 10.3354/meps08477

Sun, W., Dong, C., Tan, W., & He, Y. (2019). Statistical characteristics of cyclonic warm-core eddies and anticyclonic cold-core eddies in the North Pacific based on remote sensing data. *Remote Sensing*, *11*(2), 208. doi: 10.3390/rs11020208

Sutyrin, G., & Khain, A. (1984). Effect of the ocean-atmosphere interaction on the intensity of a moving tropical cyclone. *Izvestiya Atmospheric and Oceanic Physics*, *20*, 697–703. doi:10.1029/2007GL029683

Walker, N. D., Leben, R. R., & Balasubramanian, S. (2005). Hurricane-forced upwelling and chlorophyll a enhancement within cold-core cyclones in the Gulf of Mexico. *Geophysical Research Letters*, *32*(18), L18610. doi:10.1029/ 2005GL023716

Wang, G., Ling, Z., & Wang, C. (2009). Influence of tropical cyclones on seasonal ocean circulation in the South China Sea. *Journal of Geophysical Research: Oceans*, *114*, C10022. doi: 10.1029/2009JC005302

Wang, G., Wu, L., Johnson, N. C., & Ling, Z. (2016). Observed three-dimensional structure of ocean cooling induced by Pacific tropical cyclones. *Geophysical Research Letters*, *43*(14), 7632–7638. doi:10.1002/ 2016GL069605

Wang, X., Wang, C., Zhang, L., & Wang, X. (2015). Multidecadal variability of tropical cyclone rapid intensification in the Western North Pacific. *Journal of Climate*, *28*(9), 3806-3820. doi: 10.1175/JCLI-D-14-00400.1

Wang, Z.-F., Sun, L., Li, Q.-Y., & Cheng, H. (2019). Two typical merging events of oceanic mesoscale anticyclonic eddies. *Ocean Science*, *15*(6), 1545-1559. doi: 10.5194/os-2019-67

Yablonsky, R. M., & Ginis, I. (2009). Limitation of one-dimensional ocean models for coupled hurricane–ocean model forecasts. *Monthly Weather Review*, *137*(12), 4410-4419. doi: 10.1175/2009MWR2863.1

Zhang, H., Chen, D., Zhou, L., Liu, X., Ding, T., & Zhou, B. (2016). Upper ocean response to typhoon Kalmaegi (2014). *Journal of Geophysical Research: Oceans*, *121*(8), 6520–6535. doi:10.1002/ 2016JC012064

Zhang, Y., Zhang, Z., Chen, D., Qiu, B., & Wang, W. (2020). Strengthening of the Kuroshio current by intensifying tropical cyclones. *Science*, *368*(6494), 988–993. doi: 10.1126/science.aax5758